Resistive Switching in TaN/AlN$_x$/TiN Cell

Hsin-Ping Huang, Shyankay Jou

Abstract—Resistive switching of aluminum nitride (AlN$_x$) thin film was demonstrated in a TaN/AlN$_x$/TiN memory cell that was prepared by sputter deposition techniques. The memory cell showed bipolar switching of resistance between +3.5 V and –3.5 V. The resistance ratio of high resistance state (HRS) to low resistance state (HRS), R_{HRS}/R_{LRS}, was about 2 over 100 cycles of endurance test. Both the LRS and HRS of the memory cell exhibited ohmic conduction at low voltages and Poole-Frenkel emission at high voltages. The electrical conduction in the TaN/AlN$_x$/TiN memory cell was possibly attributed to the interactions between charges and defects in the AlN$_x$ film.

Keywords—Aluminum nitride, nonvolatile memory, resistive switching, thin films.

I. INTRODUCTION

RESISTIVE Random Access Memory (RRAM) has been extensively studied for the application in advanced nonvolatile memory [1]. In general, an RRAM cell has two resistance states that are suitable to represent ON- and OFF-states of digital signals. Typical RRAM devices are made of a sandwiched metal-insulator-metal (MIM) structure that is easy to integrate with complementary metal-oxide-semiconductor (CMOS) processes. Until now, most RRAM studies employed oxides as resistor materials [2], [3]. Recently, RRAM devices using nitride resistors, including AlN and SiN, were of interest. By utilizing various metallic electrodes with AlN resistor, bipolar switching of resistance has been demonstrated in Cu/AlN/Pt [4], Ti/AlN/Pt [5], and W/AlN/Al [6] systems. Other conductive materials such as TiN and indium tin oxide (ITO) also have been applied as electrodes in AlN-based RRAM, such as Pt/AlN/TiN [7], Cu/AlN/TiN [8], and ITO/AlN/ITO [9]. Similarly, SiN-based RRAM utilizing various electrode materials showed resistive switching behaviors. RRAM of Ag/Si$_3$N$_4$/Pt [10], Ag/Si$_3$N$_4$/Al [11], Au/Si$_3$N$_4$/Ti [12], and Ti/Si$_3$N$_4$/Ti [13] showed bipolar switching of resistance, whereas ITO/SiN/ITO exhibited unipolar switching of resistance [14].

Both aluminum nitride and silicon nitride are dielectric materials with nitride-related traps that might dominate their charge transport behaviors. Electrical conduction and resistive switching in some nitride RRAM devices were attributed to the interactions of electrical charges with nitride-related traps [5],

H.-P. Huang is with the Department of Materials Science and Engineering, National Taiwan University of Science and Technology, Taipei 106, Taiwan, ROC (e-mail: m10104307@mail.ntust.edu.tw).

S. Jou is with the Department of Materials Science and Engineering, National Taiwan University of Science and Technology, Taipei 106, Taiwan, ROC (phone: +886-2-27376665; fax: +886-2-27376544; e-mail: sjou@mail.ntust.edu.tw).

[8], [9], [11]–[13]. On the other hand, electrical conduction and resistive switching in some other nitride RRAM devices were governed by paths of metallic filaments which were generated from interactions of electrode materials and nitride resistors [4], [8], [10], [14].

Metallic nitrides such as TiN, TaN and WN have been utilized as conductive materials in CMOS technologies. TiN has also been utilized as one electrode together with another metallic electrode in AlN-based RRAM devices [7]–[8]. In our previous studies, we have employed TaN electrode in oxide-based RRAM devices [15]–[16]. In this study, we employed TiN and TaN electrodes together with an AlN$_x$ resistor to make a nitride RRAM and demonstrated bipolar switching of resistance in a TaN/AlN$_x$/TiN device. Furthermore, we correlated the structure of the AlN$_x$ film and resistive switching properties for the TaN/AlN$_x$/TiN device.

II. EXPERIMENTAL

Thin films of a TiN bottom electrode, an AlN$_x$ resistor layer and a TaN top electrode were sequentially deposited on an SiO$_2$-covered Si substrate using DC magnetron sputtering techniques. The sputtering chamber was evacuated to a pressure less than 6.7×10^{-4} Pa (5×10^{-6} torr) prior to the depositions. The depositions were conducted in flowing mixtures of Ar and N$_2$ and at ambient temperature. The sputter deposition parameters are summarized in Table I.

TABLE I
SPUTTER DEPOSITION PARAMETERS FOR NITRIDE FILMS

	TiN	AlN$_x$	TaN
DC power (W)	20	30	50
Working pressure (Pa)	0.67	0.8	0.67
Ar flow rate (cm^3/min)	15	3	18
N$_2$ flow rate (cm^3/min)	2	9	2

Structure of the blanket AlN$_x$ film was analyzed by X-ray diffraction (XRD) using Cu $K\alpha$ radiation and by transmission electron microscopy (TEM). Binding energies of the AlN$_x$ film were investigated by X-ray photoelectron spectroscopy (XPS) using Al $K\alpha$ radiation (1486.7 eV). The binding energies of Al $2p$ and N $1s$ were corrected with C $1s$ peak of 284.5 eV.

A TaN/AlN$_x$/TiN MIM structure with an 150-nm-thick TaN, a 50-nm-thick AlN$_x$ and an150-nm-thick TiN was fabricated for electrical measurements. In order to form the MIM structure, a blanket TiN layer was coated on the top of an SiO$_2$-coverd Si substrate, whereas the AlN$_x$ layer and the TaN layer were deposited through shadow masks of 2.0 mm and 0.15 mm in diameter, respectively. To study resistive switching properties of the TaN/AlN$_x$/TiN device, current–voltage (*I–V*) characterization was performed by cyclically applying DC voltages across the TaN top electrode and the TiN bottom

electrode.

III. RESULTS AND DISCUSSION

Fig. 1 shows the XRD pattern of the AlN_x film with peaks centering at diffraction angles, 2θ, of 33.3°, 36.2°, 37.9°, 50.0°, 59.5° and 66.1°, which represent reflections of (100), (002), (101), (102), (110) and (103) planes of wurtzite aluminum nitride. Fig. 2 shows the cross-sectional TEM image of the AlN_x film. The AlN_x layer is composed of crystals with clear lattice fringes as seen at the upper left to the lower right regions in Fig. 2. Other regions comprise randomly arranged atoms, indicating the presence of amorphous phase in the AlN_x film. According to the XRD and TEM analyses, the AlN_x film prepared by sputter deposition in this study is composed of a mixture of crystalline and amorphous phases.
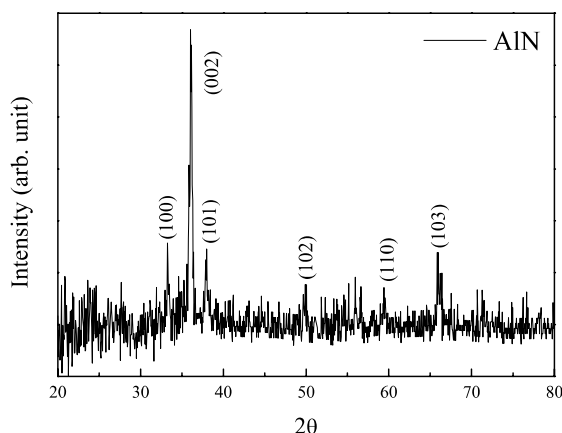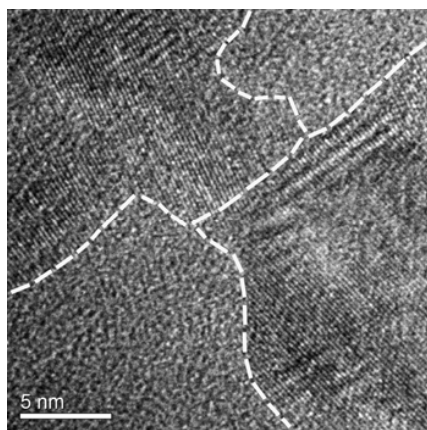

Fig. 1 XRD pattern of the AlN_x film

Fig. 2 Cross-section TEM image of the AlN_x film

The XPS analyses showed that the AlN_x film was composed of Al, N and O. According to studies of deposition and oxidation of AlN_x, the incorporation of oxygen in AlN_x was possibly due to adsorbed contamination, interaction of AlN_x film with air, or the limit of deposition condition [17]–[19]. The incorporated oxygen could substitute for nitrogen to form oxygen-related defects in AlN crystals [20], [21], or form oxynitride phase (AlO_xN_y) [22]. Fig. 3 (a) displays the XPS spectrum of Al $2p$ and two fitted peaks of the AlN_x film. The fitted Al2p #1 peak with a binding energy of 73.3eV is assigned to bound Al–N in wurtzite AlN, whereas the Al2p #2 with a binding energy of 74.9eV is assigned to Al–O bond [18], [19]. The ratio of Al–N to Al–O is about 89:11 for the AlN_x film. Further, the N 1s spectrum and two fitted peaks are shown in Fig. 3 (b). The fitted N1s#1 peak with a binding energy of 396.6eV originates from N–Al bond in wurtzite AlN, and the N1s #2 peak with a binding energy of 398.9eV can be assigned to nitrogen bound indirect to oxygen via an aluminum ion, i.e., N–Al–O bonding [19]. The ratio of Al–N to N–Al–O is about 84:16.The N–Al bond was suggested to be associated with the AlN cyrstals in the AlN_x film, whereas the N-Al-O bonds may be present in the AlN_x crystallites and on their surface [21]. On the other hand, no N 1s peak with binding energies of around 395 eV or greater than 400 eV are observed in Fig. 3 (b). Hence the AlN_x film contained no N–N and N–O bonds. According to the XRD, TEM and XPS analyses, the AlN_x film was composed of crystalline and amorphous phases with mainly Al–N bonds and some N–Al–O bonds. Therefore, nitrogen- and oxygen-related defects were present in the AlN_x film.
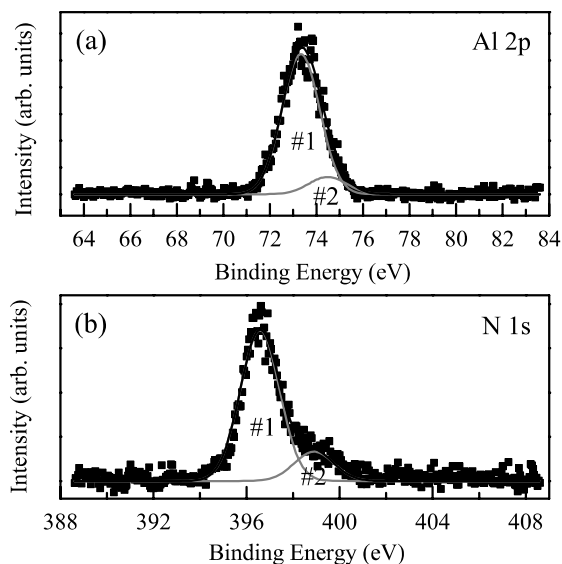

Fig. 3 XPS spectra of (a) Al $2p$ and (b) N 1s for the AlN_x film

Resistive switching was demonstrated through cyclically measuring I–V curves of the $TaN/AlN_x/TiN$ RRAM device. During the I–V measurement DC voltages were applied to the top TaN electrode while the bottom TiN electrode grounded, as displayed at the inset in Fig. 4. The RRAM device showed resistive switching behavior without needing a prior electroforming procedure in this study. Fig. 4 depicts the I–V curve of the $TaN/AlN_x/TiN$ RRAM device in the first cycle of voltage sweep. The I–V curve presents bipolar resistive switching at counterclockwise direction of +3.5 V → 0 V → –3.5 V → 0 V → +3.5 V. The as-fabricated RRAM device is in high resistance state (HRS), and then changes to low resistance state (LRS) at a SET voltage of –3.5 V. The LRS

remains until a RESET voltage of +3.5 V is applied to the RRAM device, where the RRAM device changes back to HRS. The TaN/AlN$_x$/TiN RRAM device can be reversibly switched between HRS and LRS by cyclically applying voltage sweeps.
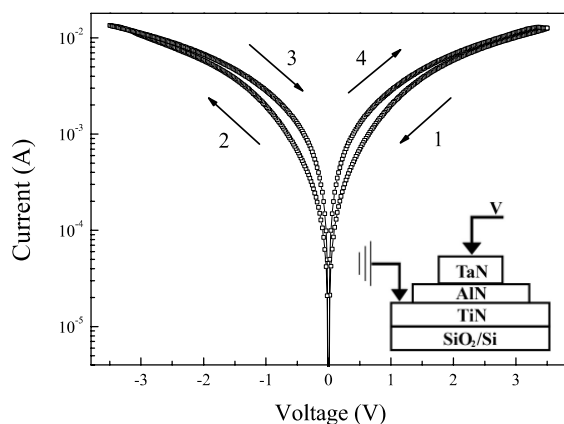

Fig. 4 *I–V* curve of the TaN/AlN$_x$/TiN RRAM device in the 1st cycle of voltage sweep. The inset is a schematic drawing of the device
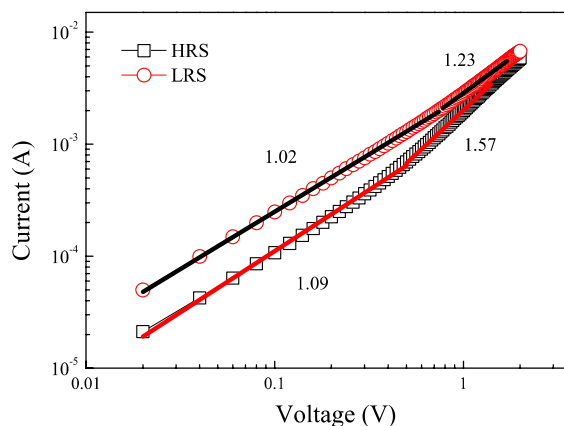

Fig. 5 Replot of *I–V* curve of the TaN/AlN$_x$/TiN RRAM device in log–log scale

To realize conduction mechanisms for the TaN/AlN$_x$/TiN RRAM device, a logarithmic plot of the *I–V* curve for the first cycle of resistive switching is depicted in Fig. 5. The slopes of the curves for both LRS and HRS are about 1 in the low-voltage region, thus the electrical conduction agrees with Ohm's law ($I \propto V$). In the high-voltage region, the slopes are greater than 1 for both LRS and HRS, thus other conduction mechanisms must be considered. Fig. 6 presents the plots of Ln (*I/V*) against $V^{1/2}$ for the LRS and HRS of the TaN/AlN$_x$/TiN device in the high-voltage region. Both plots are linear and fit with Poole-Frenkel (PF) emission model [23]. Therefore, electrical conduction of both LRS and HRS of the TaN/AlN$_x$/TiN RRAM device are divided into two sections with ohmic conduction at low voltages and PF emission at high voltages. Such combined conduction mechanism is similar to that observed in Mo/AlN/Mo capacitor with ohmic conduction at low fields and PF emission in breakdown vicinity [24].
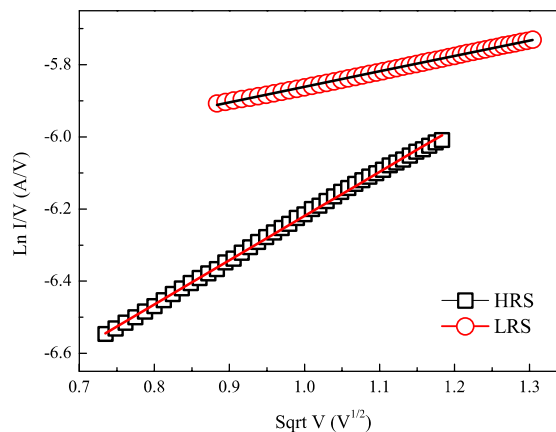

Fig. 6 Linear fitting of Ln *I/V* against $V^{1/2}$ for the TaN/AlN$_x$/TiN RRAM device in the high-voltage regions

The conduction mechanisms for the TaN/AlN$_x$/TiN RRAM device could be attributed to the interactions of electrical charges with defects in the AlN$_x$ film. Nitride-related electron traps have been suggested to dominate conducting behaviors in aluminum nitride [5], [9] and silicon nitride [11], [12], [14]. On the other hand, oxygen vacancies could be present and govern conduction in aluminum oxynitride [25]. According to the XRD, XPS and TEM analyses, the AlN$_x$ film was made of crystalline and amorphous phases of AlN and with some N–Al–O bonds. Therefore, nitride-related defects and oxygen-related defects existed in the AlN$_x$ film. These defects could facilitate charge transport via hopping conduction. At low voltages the conduction was ascribed to transport of thermally excited electrons through charge trapping process and exhibited ohmic conduction [11]. Then trap-to-trap hopping took place at high voltages via field-enhanced excitation of trapped electrons, which is known as PF emission [11]. Moreover, conductive path comprising trapped electrons could form at local region of high-density defects in LRS. Part of the conductive path was ruptured through de-trapping process and then the device was switched to HRS.

Fig. 7 shows the result of the endurance test for the TaN/AlN$_x$/TiN RRAM device by plotting the resistance data at +0.2 V for LRS and HRS. The R_{HRS}/R_{LRS} is about 2 for 100 cycles of resistive switching measurements. Both R_{HRS} and R_{LRS} increase with measurement cycles at the beginning and become stable after 60 cycles of measurements. The reason for the increase of resistance of the TaN/AlN$_x$/TiN RRAM device in the beginning of the switching measurement is not realized yet. It is suggested that the surface of the TaN top electrode would possibly react with air and form a thin insulating surface during the resistive switching measurement. This problem can be resolved by adding a passivation coating to protect the TaN top electrode in future study. However, a passivation layer for the top TaN electrode is not required in a real RRAM device because the memory cells are placed inside an IC chip with protective packaging substance.
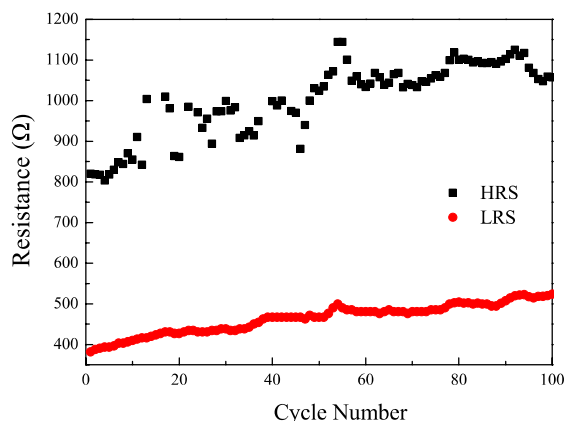
Fig. 7 Cycling endurance of the TaN/AlN$_x$/TiN RRAM device

IV. Conclusion

The resistive switching of a TaN/AlN$_x$/TiN RRAM device was inspected. The nitride RRAM device exhibited bipolar switching of resistance. The resistive switching behavior was possibly correlated with nitride-related defects and oxygen-related defects in the AlN$_x$ film.

References

[1] J. J. Yang, D. B. Strukov, and D. R. Stewart, "Memristive devices for computing," *Nature Nanotechnol.*, vol. 8, no. 1, 13–24, Jan. 2013.

[2] A. Sawa, "Resistive switching in transition metal oxides," *Mater. Today*, vol. 11, no. 6, pp. 28-36, Jun. 2008.

[3] H. S. P. Wong, H.-Y. Lee, S. Yu, Y.-S. Chen, Y. Wu, B. Lee, F. T. Chen, and M.-J. Tsai, "Metal-oxide RRAM," *Proc. IEEE*, vol. 100, no. 6, pp. 1951-1970, Jun. 2012.

[4] C. Chen, Y. C. Chang, F. Zeng, and F. Pan, "Bipolar resistive switching in Cu/AlN/Pt nonvolatile memory device," *Appl. Phys. Lett.*, vol. 97, no. 8, pp. 083502-1–083502-3, Aug. 2010.

[5] H.-D. Kim, H.-M. An, E. B. Lee, and T. G. Kim, "Stable resistive switching characteristics and resistive switching mechanisms observed in aluminum nitride-based ReRAM devices," *IEEE Trans. Electron Devices*, vol. 58, no. 10, pp. 3566–3573, Oct. 2011.

[6] M. J. Marinella, J. E. Stevens, E. M. Longoria, and P. G. Kotula, "Resistive switching in aluminum nitride," in *Dig. 70th Annual Device Research Conf.*, University Park, TX, 2012, pp. 89–90.

[7] B. J. Choi, J. J. Yang, M.-X. Zhang, K. J. Norris, D. A. A. Ohlberg, N. P. Kobayashi, G. Medeiros-Ribeiro, and R. S. Williams, "Nitride memristors," *Appl. Phys. A*, vol. 109, no. 1, pp. 1–4, Oct. 2012.

[8] C. Chen, S. Gao, G. Tang, H. Fu, G. Wang, C. Song, F. Zeng, and F. Pan, "Effect of electrode materials on AlN-based bipolar and complementary resistive swithching," *ACS Appl. Mater. Interfaces*, vol 5, no. 5, pp. 1793-1799, 2013.

[9] H.-D. Kim, H.-M. An, Y. Seo, and T. G. Kim, "Transparent resistive switching memory using ITO/AlN/ITO capacitor," *IEEE Electron Device Lett.*, vol. 32, no. 8, pp. 1125–1127, Aug. 2011.

[10] B. Sun, L. F. Liu, Y. Wang, D. D. Han, X. Y. Liu, R. Q. Han, and J. F. Kang, "Bipolar resistive switching behaviors of Ag/Si$_3$N$_4$/Pt memory device," in *Proc.9th Int. Conf. Solid-State and Integrated-Circuit Tech.*, Beijing, 2008, pp. 925–927.

[11] H.-D. Kim, H.-M. An, K. C. Kim, Y. Seo, K.-H. Nam, H.-B. Chung, E. B. Lee, and T. G. Kim, "Large resistive-switching phenomena observed in Ag/Si$_3$N$_4$/Al memory cells," *Semicond. Sci. Technol.*, vol. 25, no. 6, pp. 065002-1–065002-5, Jun. 2010.

[12] H.-D. Kim, H.-M. An, and T. G. Kim, "Improved reliability of Au/Si$_3$N$_4$/Ti resistive switching memory cells due to a hydrogen postannealing treatment," *J. Appl. Phys.*, vol. 109, no. 1, pp. 016105-1–016105-3, Jan. 2010.

[13] H.-D. Kim, H.-M. and An, and T. G. Kim, "Resistive switching behavior in Ti/Si$_3$N$_4$/Ti memory structures for ReRAM application," *Microelectron. Eng.*, vol. 98, pp. 351–354, Oct. 2012.

[14] H.-D. Kim, H.-M. An, S. M. Hong, and T. G. Kim, "Unipolar resistive switching phenomena in fully transparent SiN-based memory cells," *Semicond. Sci. Technol.*, vol. 27, no. 12, pp. 125020-1–125020-6, Dec. 2012.

[15] S. Jou and M.-E. Han, "Influence of interfacial tantalum oxynitride on resistive switching of Cu/Cu-SiO$_2$/TaN," *Jpn. J. Appl. Phys.*, vol. 51, no. 5., pp. 055701-1–055701-4, May 2012.

[16] S. Jou and C.-L. Chao, "Resistance switching of copper-doped tantalum oxide prepared by oxidation of copper-doped tantalum nitride," *Surf. Coat. Technol.*, vol. 231, pp. 311-315, Sep. 2013.

[17] X.-D. Wang, K. W. Hipps, and U. Mazur, "Infrared and morphological studies of hydrogenated AlN thin film," *Langmuir*, vol. 8, no. 5, pp. 1347-1353, May 1992.

[18] A. Mahmood, N. Rakov, and M. Xiao, "Influence of deposition conditions on optical properties of aluminum nitride (AlN) thin films prepared by DC-reactive magnetron sputtering," *Mater. Lett.*, vol. 57, no. 13–14, pp. 1925-1933, Apr. 2003.

[19] L. Rosenberger, R. Baird, E. McCullen, G. Auner, and G. Shreve, "XPS analysis of aluminum nitride films deposited by plasma source molecular beam epitaxy," *Surf. Interface. Anal.*, vol. 40, no. 9, pp. 1254-1261, Sep. 2008.

[20] D. Chen, J. Wang, D. Xu, and Y. Zhang, "The influence of defects and impurities in polycrystalline AlN films on the violet and blue emission," *Vacuum*, vol. 83, no. 5, pp. 865–868,Jan. 2009.

[21] J. H. Harris, R. A. Youngman, and R. G. Teller, "On the nature of oxygen-related defect in aluminum nitride," *J. Mater. Res.*, vol. 5, no. 8, pp. 1768–1773, Aug. 2008.

[22] C. K. Hwangbo, L. J. Lingg, J. P. Lehan, H. A. Macleod, and F. Suits, "Reactive ion assisted deposition of aluminum oxynitride thin films," *Appl. Opt.*, vol. 28, no. 14, pp. 2779–2784, Jul. 1989.

[23] P. C. Joshi and B. Krupanidhi, "Structural and electrical characteristics of SrTiO$_3$ thin films for dynamic random access memory applications," *J. Appl. Phys.*, vol. 73, no. 11, pp. 7627-7634, Jun. 1993.

[24] N. B. Hassine, D. Mercier, P. Renaux, G. Parat, S. Basrour, P. Waltz, C. Chappaz, P. Ancey, and S. Blonkowski, "Dielectrical properties of metal-insulator-metal aluminum nitride structures: measurement and modeling," *J. Appl. Phys.*, vol. 105, no.4 , pp. 044111-1–044111-10, Feb. 2009.

[25] N. H. Chen, Z. W. Zheng, C. H. Cheng, and F. S. Yeh, "Sub-micro watt resistive memories using nano-crystallized aluminum oxynitride dielectric," Appl. Phys. A., published online, Dec. 2013.